Multi-Temperature Crystallographic Studies of Mixed-Valence Polynuclear Complexes; Valence Trapping Process in the Trinuclear Oxo-Bridged Iron Compound, $[Fe_3O(O_2CC(CH_3)_3)_6(C_5H_5N)_3]$

Claire Wilson,[†,⊥] Bo B. Iversen,*[,†] Jacob Overgaard,[†] Finn K. Larsen,[†] Guang Wu,[‡] Sergiu P. Palii,[§] Grigore A. Timco,[§] and Nicolae V. Gerbeleu[§]

Department of Chemistry, University of Aarhus, DK-8000 Aarhus C, Denmark, National Synchrotron Light Source, Brookhaven National Laboratory, Upton, New York 11973, USA, and Institute of Chemistry, Academy of Sciences of the Republic of Moldova, Chisinau, MD-2028, Moldova

Received November 29, 1999

Abstract: Single-crystal X-ray diffraction data have been collected on five different crystals at 12 different temperatures (10, 28, 35, 60, 85, 100, 118, 135, 160, 200, 240, 295 K) on a trinuclear, oxo-bridged, mixed-valence iron complex, $Fe_3O(O_2CC(CH_3)_3)_6(C_5H_5N)_3$, using both synchrotron and conventional radiation sources. The present study for the first time provides structural information for an oxo-bridged trinuclear compound below the boiling point of nitrogen (77 K). The use of very low-temperature crystallographic data is crucial for understanding the physical properties of the complex. No change of space group is observed in the whole temperature range, although a reversible broadening of the Bragg peaks is observed around 85 K. The structure has ordering processes involving the *tert*-butyl groups, and above 85 K, four *tert*-butyl groups become disordered. Around 150 K, a fifth *tert*-butyl becomes disordered, whereas the last *tert*-butyl is ordered at all temperatures. Very significant temperature-dependent changes in the Fe-ligand bond lengths are observed which are interpreted as being due to dynamic disorder caused by intramolecular electron transfer (ET) between the metal sites. The ET process is significantly affected by changes in the molecular potential energy surface (PES) caused by the dynamic behavior of the *tert*-butyls. The dynamic disorder of the Fe_3O core resulting from the ET process is examined through analysis of the atomic displacement parameters. The ET process involves only two of the three iron sites, with the third site appearing to be valence-trapped at all temperatures. The trapping of this iron site at all temperatures appears to be related to the asymmetry caused by the different dynamic behaviors of the *tert*-butyls. At very low temperatures (<10 K), the system becomes valence-trapped and consists of a single configuration without disorder. Boltzmann population models are used to estimate the energy difference between the two lowest-lying minima on the PES ($\Delta E < 100$ cm^{-1}) and between two disordered configurations of each of the *tert*-butyls ($\Delta E = 217$, 212, 255, 359, and 345 cm^{-1}).

1. Introduction

Polynuclear transition-metal complexes occur widely in nature, and their study spans fields ranging from biology to photophysics.[1] In the case of intramolecular electron transfer (ET) processes, the trinuclear mixed-valence compounds of the type $[M_3O(O_2CR)_6L_3]\cdot n$S (where M = metal atom, L = terminal monodentate ligand, S = solvent molecule of crystallization) have been intensively investigated.[2] In particular, studies have been carried out on trinuclear mixed-valence iron systems $[Fe^{III}{}_2Fe^{II}O(O_2CR)_6L_3]\cdot n$S, which have the advantage of allowing the use of Mössbauer spectroscopy as well as other techniques to investigate the factors that affect the rate of this intramolecular ET process.[2,3] The first compound of this class that has been characterized in detail, $[Fe_3O(O_2CCH_3)_6(H_2O)_3]\cdot 2H_2O$, was synthesized by Chrétien and Lous in 1944,[4] while temperature-dependent studies of trinuclear mixed-valence iron species were initiated in the works of Lupu et al.[5] and Turta et al.[6] by employing Mössbauer spectroscopy and magnetochemistry. Previously, we studied a number of trinuclear iron complexes by similar methods.[7] Generally, the many possible combinations of carboxylate bridges (RCOO), ligands (L), and solvates (S) allow systematic studies to be made, thereby allowing the effect of each of these factors to be examined.

Variable-temperature IR studies have established that most compounds studied are, at least partially, valence-localized complexes.[2,3c] However, many of the systems show temperature-dependent Mössbauer spectra, changing from a trapped (ET is slow on the Mössbauer time scale, $\sim 10^7$ s^{-1}) to a detrapped system on raising the temperature. Hendrickson and co-workers have demonstrated that solvate molecules in the crystal, by both their presence and nature, can have a marked effect on the rate of intramolecular ET.[3f] For example, the compound $[Fe_3O(O_2CCH_3)_6(C_5H_5N)_3]\cdot$S remains trapped up to 315 K when unsolvated, whereas the solvated complexes become detrapped as the temperature is raised but show different temperature dependence for S = C_5H_5N and S = C_6H_6.[3f] One or more phase transitions have been observed in many of these systems, and it has been suggested that the valence-trapping process is

* Corresponding author. E-mail: bo@kemi.aau.dk.
† University of Aarhus.
‡ Brookhaven National Laboratory.
§ Academy of Sciences of the Republic of Moldova.
⊥ Present address: School of Chemistry, University of Nottingham, Nottingham, NG7 2RD, U.K.

(1) Lippard, S. J. *Angew. Chem., Int. Ed. Engl.* **1988**, *27*, 344−361.
(2) Cannon, R. D.; White, R. P. *Prog. Inorg. Chem.* **1988**, *36*, 195−297.

10.1021/ja994162a CCC: $19.00
Published on Web 11/01/2000

connected to an order−disorder phase transition involving the solvate molecules.[3h] It has been proposed that the disordered solvate molecules provide a more symmetrical environment for the metal sites, thus facilitating ET.[3h] However, it is not always clear that the phase transitions are directly connected to the ET process. In recent years, there have been a number of systems reported which undergo a valence-trapping process, but which are unsolvated.[3t,3x] It has been suggested that long ligand chains could impose a similar order−disorder-type behavior as solvate molecules,[3t] but subsequent studies without bulky groups or free solvate molecules in the crystal still showed that valence trapping was occurring.[3x] Therefore, it appears that, although solvate molecules affect the valence-trapping process, additional factors can be involved.

In this paper, we present the results of variable-temperature crystallographic studies of the nonsolvated mixed-valence complex $[Fe_3O(O_2CC(CH_3)_3)_6(C_5H_5N)_3]$, (**1**) (Figure 1). Full X-ray crystallographic data were measured at 12 temperatures in the range of 10−295 K (10, 28, 35, 60, 85, 100, 118, 135, 160, 200, 240, and 295 K). It is striking that even though a very large amount of literature exists concerning trinuclear complexes, no crystallographic information is available on such complexes below the boiling point of nitrogen (77 K). It is demonstrated that very low-temperature structural information facilitates additional characterization of the system. The room-temperature structure and some spectroscopic properties of **1** were recently reported by Wu et al.[3y] It was suggested that ET takes place between only two of the iron sites, while the third site remains trapped formally as $Fe^{(III)}$ at all temperatures. Using synchrotron radiation-resonance scattering on **1**, a link later was established between the formal oxidation states of the Fe atoms and the Fe-ligand bond lengths.[8] In the present paper, we take advantage of the large amount of information that is contained in temperature-resolved crystallographic data and examine the structure in detail. This provides information about the ET process as well as the shape of the potential energy surface.

2. Experimental Section

2.1 Synthesis. $[Fe_3O(O_2CC(CH_3)_3)_6(HO_2CC(CH_3)_3)_3]$ (A). Finely dispersed iron, 2.0 g, in pivalic acid ($HO_2CC(CH_3)_3$), 30 mL, was heated at 155−160 °C in the presence of air up to practically complete dissolution of iron (caution: hydrogen is released). After cooling to room temperature, the obtained precipitate was dissolved by refluxing in diethyl ether, 50 mL, filtered and evaporated to ∼40 mL. The dark-brown solution was put into a cooler at 10 °C. The big dark-brown hexagonal crystals, which are sedimented, were filtered after 24 h in inert atmosphere, were washed with a small quantity of cooled diethyl ether and with acetonitrile, and were dried at room temperature. All manipulations of crystals (including storage) were carried out in inert atmosphere. Yield: 6.0 g. Anal. Calc. for $C_{45}H_{84}O_{19}Fe_3$: C, 49.28; H, 7.72; Fe, total 15.28; $Fe^{(II)}$, 5.09. Found: C, 49.05; H, 7.60; Fe, total 15.40; $Fe^{(II)}$, 5.08.

$[Fe_3O(O_2CC(CH_3)_3)_6(C_5H_5N)_3]$ (1). Compound **A**, 4 g, was dissolved in pyridine (C_5H_5N), 10 mL, in inert atmosphere by heating. After filtration, the hot solution was cooled slowly and left 48 h at room temperature. The precipitated black crystals were collected, washed with small quantities of cooled pyridine and acetonitrile, and dried at room temperature in inert atmosphere. The complex is very stable in air (after 12 years, the crystals were still suitable for X-ray analysis). Anal. Calc. for $C_{45}H_{69}N_3O_{19}Fe_3$: C, 52.60; H, 6.77; N, 4.09; Fe, total 16.30; $Fe^{(II)}$, 5.43. Found: C, 52.13; H, 6.85; N, 4.19; Fe, total 16.33; $Fe^{(II)}$, 5.40.

Analysis. The metal content was determined using the method of Charlot.[9] Total iron content was determined by dissolving the complex while heating in HCl (concentrated), followed by reduction with excess of tin(II) chloride, oxidation of the excess of the latter with mercury-(II) chloride, and titration in the presence of phosphoric acid with potassium dichromate, employing diphenylamino-sulfonate as an indicator. Iron(II) content was determined by dissolving the complex in sulfuric acid, 6N, and titration with potassium dichromate as described above.

(3) (a) Dziobkowski, C. T.; Wrobleski, J. T.; Brown, D. B. *Inorg. Chem.* **1981**, *20*, 679−684. (b) Cannon, R. D.; Montri, L.; Brown, D. B.; Marshall, K. M.; Elliot, C. M. *J. Am. Chem. Soc.* **1984**, *106*, 2591−2594. (c) Meesuk, L.; Jayasooriya, U. A.; Cannon, R. D. *J. Am. Chem. Soc.* **1987**, *109*, 2009−2016. (d) White, R. P.; Wilson, L. M.; Williamson, D. J.; Moore, G. R.; Jayasooriya, U. A.; Cannon, R. D. *Spectrochim. Acta Sect. A* **1990**, *46*, 917−920. (e) White, R. P.; Stride, J. A.; Bollen, S. K.; Sa-Ard, N. C.; Kearley, G. J.; Jayasooriya, U. A.; Cannon, R. D. *J. Am. Chem. Soc.* **1993**, *115*, 7778−7782. (f) Oh, S. M.; Hendrickson, D. N.; Hassett, K. L.; Davis, R. E. *J. Am. Chem. Soc.* **1985**, *107*, 8009−8018. (g) Woehler, S. E.; Wittebort, R. J.; Oh, S. M.; Hendrickson, D. N.; Inniss, D.; Strouse, C. E. *J. Am. Chem. Soc.* **1986**, *108*, 2938−2946. (h) Sorai, M.; Kaji, K.; Hendrickson, D. N.; Oh, S. M. *J. Am. Chem. Soc.* **1986**, *108*, 702−708. (i) Oh, S. M.; Wilson, S. R.; Hendrickson, D. N.; Woehler, S. E.; Wittebort, R. J.; Inniss, D.; Strouse, C. E. *J. Am. Chem. Soc.* **1987**, *109*, 1073−1090. (j) Woehler, S. E.; Wittebort, R.; Oh, S. M.; Kambara, T.; Hendrickson, D. N.; Inniss, D.; Strouse, C. E. *J. Am. Chem. Soc.* **1987**, *109*, 1063−1072. (k) Jang, H. G.; Geib, S. J.; Kaneko, Y.; Nakano, M.; Sorai, M.; Rheingold, A. L.; Montez, B.; Hendrickson, D. N. *J. Am. Chem. Soc.* **1989**, *111*, 173−186. (l) Sorai, M.; Shiomi, Y.; Hendrickson, D. N.; Oh, S. M.; Kambara, T. *Inorg. Chem.* **1987**, *26*, 223−230. (m) Nakano, M.; Sorai, M.; Vincent, J. B.; Christou, G.; Jang, H. G.; Hendrickson, D. N. *Inorg. Chem.* **1989**, *28*, 4608−4614. (n) Kaneko, Y.; Nakano, M.; Sorai, M.; Hendrickson, D. N. *Inorg. Chem.* **1989**, *28*, 1067−1073. (o) Jang, H. G.; Kaji, K.; Sorai, M.; Wittebort, R. J.; Geib, S. J.; Rheingold, A. L.; Hendrickson, D. N. *Inorg. Chem.* **1990**, *29*, 3547−3556. (p) Jang, H. G.; Wittebort, R. J.; Sorai, M.; Kaneko, Y.; Nakano, M.; Hendrickson, D. N. *Inorg. Chem.* **1992**, *31*, 2265−2271. (q) Wu, C. C.; Jang, H. G.; Rheingold, A. L.; Gutlich, P.; Hendrickson, D. N. *Inorg. Chem.* **1996**, *35*, 4137−4147. (r) Wu, C. C.; Hunt, S. A.; Gantzel, P. K.; Gutlich, P.; Hendrickson, D. N. *Inorg. Chem.* **1997**, *36*, 4717−4733. (s) Manchanda, R. *Inorg. Chim. Acta* **1996**, *245*, 91−95. (t) Nakamoto, T.; Katada, M.; Kawata, S.; Kitagawa, S.; Kikuchi, K.; Ikemoto, I.; Endo, K.; Sano, H. *Chem. Lett.* **1993**, 1463−1466. (u) Asamaki, K.; Nakamoto, T.; Kawat, S.; Sano, H.; Katada, M.; Endo, K. *Inorg. Chim. Acta* **1995**, *236*, 155−161. (v) Sato, T.; Ambe, F.; Endo, K.; Katada, M.; Maeda, H.; Nakamoto, T.; Sano, H. *J. Am. Chem. Soc.* **1996**, *118*, 3450−3458. (x) Nakamoto, T.; Hanaya, M.; Katada, M.; Endo, K.; Kitagawa, S.; Sano, H. *Inorg. Chem.* **1997**, *36*, 4347−4359. (y) Wu, R.; Poyraz, M.; Sowrey, F. E.; Anson, C. E.; Wocadlo, S.; Powell, A. K.; Jayasooriya, U. A.; Cannon. R. D.; Nakamoto, T.; Katada, M.; Sano, H. *Inorg. Chem.* **1998**, *37*, 1913−1921. (z) Gorun, S. M.; Papaefthymiou, G. C.; Frankel, R. B.; Lippard, S. J. *J. Am. Chem. Soc.* **1987**, *109*, 4244−4255.

(4) Chrétien, A.; Lous, E. *Bull. Soc. Chim. Fr.* **1944**, *11*, 446.

(5) (a) Lupu, D. *Rev. Roum. Chim.* **1970**, *15*, 417−422. (b) Lupu, D.; Ripan, R. *Rev. Roum. Chim.* **1971**, *16*, 43−44. (c) Grecu, R.; Lupu, D. *Rev. Roum. Chim.* **1971**, *16*, 1811−1817; *Chem. Abstr. 76*: 78961c. (d) Lupu, D.; Barb, D.; Filoti, G.; Morariu, M.; Tarina, D. *J. Inorg. Nucl. Chem.* **1972**, *34*, 2803−2810; *Chem. Abstr. 77*: 120504d.

(6) (a) Gol'danskii, V. I.; Alekseev, V. P.; Stukan, R. A.; Turta, K. I.; Ablov, A. V. *Dokl. Akad. Nauk SSSR.* **1973**, *213*, 867−870 (in Russian); *Chem. Abstr. 80*: 76375y. (b) Gol'danskii, V. I.; Alekseev, V. P.; Stukan, R. A.; Turta, K. I.; Ablov, A. V. *Fiz. Mat. Metody Koord. Khim., Tezisy Dokl., Vses. Soveshch. 5th*; Shtiintsa: Kishinev, USSR, 1974; p 127 (*in Russian*); *Chem. Abstr. 83*: 35258f. (c) Goldanskii, V. I.; Ablov, A. V.; Stukan, R. A.; Borshch, S. A.; Turta, C. I.; Bobkova, S. A. *Proc. Int. Conf. Moessbauer Spectrosc.* Bucharest, Romania **1977**; vol. 1, p 221. (d) Turta, C. I.; Borshch, S. A.; Bobkova, S. A. *Proc. Int. Conf. Moessbauer Spectrosc.* Portoroj, Yugoslavia **1979**; p 127. (e) Stukan, R. A.; Turta, K. I.; Ablov, A. V.; Bobkova, S. A. *Russ. J. Coord. Chem.* **1979**, *5*, 95−102 (in Russian); *Chem. Abstr. 90*: 132073u. (f) Turta, C. I.; Bobkova, S. A.; Stratulat, G. V. *Izv. Akad. Nauk Mold. SSR, Ser. Biol. Khim. Nauk.* **1981**, *1*, 67−74. (g) Turta, K. I.; Bobkova, S. A.; Stukan, R. A.; Shova S. G. *Russ. J. Coord. Chem.* **1981**, *7*, 1682−1691 (in Russian); *Chem. Abstr. 96*: 134740g. (h) Turte, K. I.; Bobkova, S. A.; Stukan, R. A.; Dorogan, A. V.; Veksel'man, M. E. *Russ. J. Coord. Chem.* **1982**, *8*, 794−800 (in Russian); *Chem. Abstr. 97*: 137604x. (i) Turte, K. I.; Bobkova, S. A.; Stukan, R. A. *Zh. Neorg. Khim.* **1984**, *29*, 731−734 (in Russian); *Chem. Abstr. 100*: 182654e.

(7) (a) Gerbeleu, N. V.; Bobkova, S. A.; Popovich, G. A.; Timko, G. A.; Turta, K. I. *Abstracts of the VIIIth All-Union Conf. "Physical and Mathematical Methods in Coordination Chemistry". Chisinau, Moldova.* 1983; pp 162−163. (b) Gerbeleu, N. V.; Timko, G. A.; Turta, K. I.; Popovich, G. A.; Bobkova, S. A.; Indrichan, K. M. *Zh. Neorg. Khim.* **1986**, *31*, 684−690 (in Russian); *Chem. Abstr. 104*: 218065n.

(8) Wu, G.; Zhang, Y.; Ribaud, L.; Coppens, P.; Wilson, C.; Iversen, B. B.; Larsen, F. K. *Inorg. Chem.* **1998**, *37*, 6078−6083.

(9) Charlot, G. *Les Methodes de la Chimie Analitique. Analyse Quantative Minerale*; Masson Publishers: Paris, 1961.

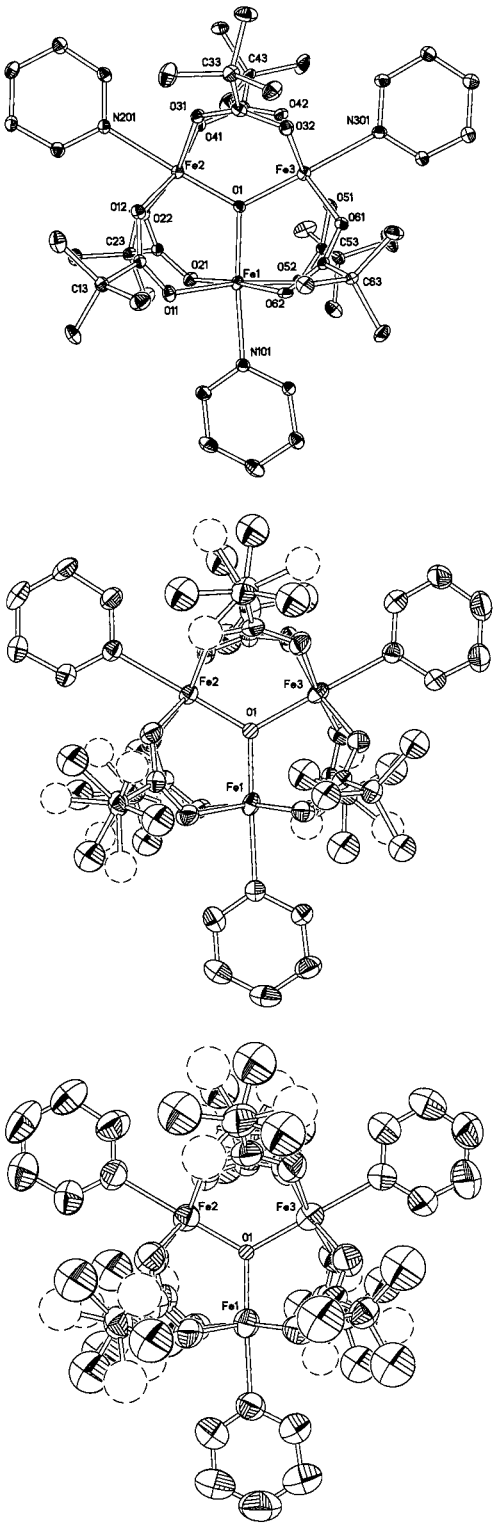

Figure 1. ORTEP drawings at the 50% probability level of the molecular structure of $[Fe_3O(O_2CC(CH_3)_3)_6(C_5H_5N)_3]$: (a) 10 K, (b) 135 K, and (c) 295 K. The minor components of the disordered *tert*-butyl groups are denoted by broken lines.

2.2 X-ray Data. Single crystal diffraction data were collected at 12 temperatures ranging from 10 to 295 K on five different crystals. A preliminary room-temperature study was made to assess crystal quality, to determine the structure, and to assess the suitability of the system for further study. A second data collection was made at room temperature as the final data set of a series. All details that are given for 295 K refinements refer to this second data set. When cooled below 85 K, many of the Bragg peaks broadened significantly but could not be resolved into separate peaks. The effect is fully reversible. No loss of symmetry of the diffracted intensities was observed, and the space group remains $P2_1$ both above and below this temperature. For the very extensive 28 K synchrotron data set, the E-statistics were 0.63, 0.83, and 0.73 for 0*kl*, *h*0*l* and *hk*0 reflections respectively, which clearly indicates an acentric space group ($\langle E \rangle_{\text{acentric}} = 0.74$, $\langle E \rangle_{\text{centric}} = 0.97$). A summary of crystallographic data is given in Table 1. Below a brief description of the experimental conditions is given.

Crystal 1: 10, 60, 85, 100, 135, 200, and 295 K. A dark red-brown single crystal of dimensions 0.35 × 0.24 × 0.24 mm, mounted inside a capillary tube with a tiny amount of vacuum grease, was used for the measurements. The preliminary room-temperature study and subsequent data collections at 10 and 60 K were made on a type-512 HUBER four-circle diffractometer equipped with a type-CS202 DISPLEX closed-cycle He-cryostat at the Department of Chemistry, University of Aarhus. Unit cell parameters at 10 K were obtained by least-squares fit to the setting angles of 25 reflections with $20° < 2\theta < 24°$, and those at 60 K by using 26 reflections with $30° < 2\theta < 36.5°$. Data were collected with graphite-monochromated Ag Kα radiation ($\lambda = 0.5608$ Å), using $\omega/2\theta$ scans, for the quadrant $-h + k \pm l$. Three standard reflections were monitored every 50 reflections. Data were reduced using the local KRYSTAL program package.[10] Integration was performed with the $\sigma(I)/I$ method,[11] and equivalent reflections were averaged using the program SORTAV.[12] Measurements at the other temperatures were made using Mo Kα radiation and narrow (0.2−0.3°) ω-scans on a Bruker AXS SMART CCD diffractometer equipped with an Oxford Cryosystems N_2-flow Cryostream cooling device at the Department of Chemistry, University of Aarhus. Diffractometer control, unit-cell parameter refinements and peak integrations were carried out using the SMART software. Equivalent reflections were scaled and averaged using the SORTAV program.[12] For all data sets, the intensities were corrected for Lorentz-polarization effects and an integration method absorption correction was made using the face-indexed description of the crystal.

Crystal 2: 160, 240 K. A crystal of approximate dimensions 0.38 × 0.31 × 0.24 mm was mounted in an oil film on a nylon fiber. Measurements were carried out on a Bruker AXS SMART CCD diffractometer at the Department of Chemistry, University of Durham, using the same procedures as for crystal 1. Empirical absorption correction and data averaging was carried out using SADABS.[13]

Crystal 3: 35 K. A crystal of dimensions similar to those of crystal 2 was mounted in an oil film on a nylon fiber. The crystal was cooled to 35 K using a controllable Oxford cryosystems open flow He gas cryostat mounted on a Bruker AXS SMART CCD diffractometer at the Department of Chemistry, University of Durham.[14] Empirical absorption correction and data averaging was carried out using SADABS.[13]

Crystal 4: 118 K. A crystal of dimensions similar to those of crystal 2 was used. Data were collected on a Bruker AXS SMART CCD diffractometer at the Department of Chemistry, the Technical University of Denmark, using the same procedures as for crystal 1, but no absorption correction was applied.

Crystal 5: 28 K. Very extensive data were collected on a crystal of maximum dimensions 100 μm at the SUNY beamline X3A1 at the NSLS, Brookhaven National Laboratory, using a Bruker CCD detector. Full experimental details will be given in a forthcoming paper on the electron density distribution of the complex.[15] The use of extremely intense synchrotron radiation allows us to determine with greater certainty if any space group changes occur at low temperatures.

(10) Hazell, A. C. *KRYSTAL − A Suite of Crystallographic Programs for Data Reduction and Refinement*; Department of Chemistry, University of Aarhus, DK − 8000 Århus C, Denmark.

(11) Lehman, M. S.; Larsen, F. K. *Acta Crystallogr. Sect A.* **1974**, *30*, 580−584.

(12) Blessing, R. *J. Appl. Crystallogr.* **1989**, *22*, 396−397.

(13) SHELXTL, version 5; Siemens Industrial Automation, Inc: Madison, WI, 1994.

(14) Goeta, A. E.; Thompson, L. K.; Sheppard, C. L.; Tandon, S. S.; Lehmann, C. W.; Cosier, J.; Webster, C.; Howard, J. A. K. *Acta Crystallogr. Sect C.* **1999**, *55*, 1243−1246.

(15) Overgaard, J.; Iversen, B. B.; Wilson, C.; Larsen, F. K.; Wu, G.; Palii, S. P.; Timco, G. A. In preparation.

Table 1. Crystallographic Data

	temp, K											
	10	28	35	60	85	100	118	135	160	200	240	295
radiation	Ag Kα	sync.	Mo Kα	Ag Kα	Mo Kα	Mo Kα	Mo Kα	Mo Kα	Mo Kα	Mo Kα	Mo Kα	Mo Kα
λ (Å)	0.56080	0.643	0.71073	0.56080	0.71073	0.71073	0.71073	0.71073	0.71073	0.71073	0.71073	0.71073
a (Å)	11.574(3)	11.583(1)	11.573(2)	11.588(3)	11.602(3)	11.608(3)	11.6346(4)	11.628(2)	11.667(1)	11.697(2)	11.765(1)	11.824(2)
b (Å)	19.732(4)	19.729(1)	19.725(4)	19.709(4)	19.748(4)	19.764(4)	19.8067(6)	19.843(4)	19.918(4)	20.018(4)	20.159(2)	20.271(4)
c (Å)	11.853(3)	11.850(1)	11.847(2)	11.875(3)	11.914(3)	11.938(2)	11.9520(3)	11.962(2)	11.981(3)	11.978(3)	12.014(1)	12.011(2)
β (deg)	106.583(1)	106.527(1)	106.469(9)	106.960(1)	106.826(1)	106.869(5)	106.903(1)	106.886(4)	106.786(3)	106.903(5)	106.880(2)	106.983(4)
V (Å^3)	2594(1)	2596(1)	2593.5(9)	2594(1)	2613(1)	2620.9(9)	2635.3(1)	2641.0(8)	2665.6(9)	2684(1)	2726.6(4)	2753.3(8)
space group	$P2_1$(No. 4)	$P2_1$ No. 4)	$P2_1$(No. 4)	$P2_1$(No. 4)	$P2_1$(No. 4)	$P2_1$(No. 4)	$P2_1$(No. 4)	$P2_1$(No. 4)	$P2_1$(No. 4)	$P2_1$(No. 4)	$P2_1$(No. 4)	$P2_1$(No. 4)
Z	2	2	2	2	2	2	2	2	2	2	2	2
D_{calc} g cm^{-3}	1.315	1.313	1.316	1.316	1.306	1.302	1.295	1.292	1.280	1.272	1.252	1.239
N_{obs}	5996	130460	10827	7393	33973	17324	17917	17395	34024	17372	34305	17591
N_{unique}	5775	18888	6578	5681	11343	11489	12289	11534	14499	11530	14891	10140
R_{int}	0.05	0.03	0.04	0.08	0.03	0.04	0.05	0.03	0.04	0.04	0.05	0.04
(sin $\theta/\lambda)_{max}$ (Å^{-1})	0.654	1.02	0.625	0.632	0.695	0.689	0.694	0.689	0.703	0.689	0.713	0.689
wR(F_o^2)	0.1488	0.0828	0.0797	0.1695	0.0856	0.0740	0.1128	0.0955	0.1095	0.12962	0.1205	0.1123
$R(F_o)$	0.0608	0.0436	0.0348	0.0685	0.0345	0.0309	0.0492	0.0371	0.0515	0.0483	0.0579	0.0544
GoF	1.36	1.72	1.07	1.22	1.15	1.06	1.27	1.24	1.03	1.07	1.17	1.34
N_{par}	577	576	579	577	578	578	577	550	550	535	527	528
μ (mm^{-1})	0.466	N/A	0.888	0.466	0.881	0.878	0.874	0.872	0.864	0.858	0.844	0.836
min/max transmission	0.893/ 0.911	N/A	0.606/ 0.647	0.894/ 0.916	0.780/ 0.847	0.762/ 0.850	N/A	0.764/ 0.851	0.474/ 0.530	0.747/ 0.850	0.479/ 0.533	0.728/ 0.856

Furthermore, the synchrotron data were recorded on a separate crystal at a temperature close to one of the conventional data sets. This allows us to better assess systematic errors in the results.

2.3 Structure Solution and Refinements. The structure was solved by direct methods followed by difference Fourier syntheses.[13] All refinements were made using program SHELXTL[13] except for those of the 28 K synchrotron data, which were carried out using program XD.[16] Positional and anisotropic thermal parameters were refined for all non-hydrogen atoms. Above 135 K, certain carbon atoms in the pivalic acid bridges were disordered and, therefore, modeled as two partly occupied sites. Hydrogen atoms were placed at calculated positions. Atomic scattering factors were taken from International Tables of Crystallography (Vol. C, Tables 4.2.6.8 and 6.1.1.4). The space group was determined to be $P2_1$ from the systematically absent reflections $0k0$ for $k \neq 2n$ and from the indication from the statistics that the space group was chiral, thus ruling out $P2_1/m$. A Flack parameter checking that the correct handedness had been chosen was refined in all cases.[17] The values ranged between $-0.06(5)$ and $0.02(2)$, and none were different from the expected value of zero. It is notable that all five different crystals examined have the same handedness. This may suggest that only one enantiomer is present in the crystalline samples.

3. Results and Discussion

3.1 Temperature dependence of the structure.. The structure of the "basic carboxylate", **1**, consists of the well-known arrangement of three Fe atoms linked by a central μ^3-O atom and further bridged by two pivalate groups between each pair of iron atoms. The octahedral coordination of each Fe atom is completed by a pyridine ligand that is nearly coplanar with the central Fe_3O core. All three iron sites are crystallographically independent. There is no solvate included in the lattice, and there is one molecule in the asymmetric unit (Figure 1). Because the complex is neutral, the three iron atoms formally carry a combined charge of +8e, and thus, formally, there are two $Fe^{(III)}$ sites and one $Fe^{(II)}$ site. Electron counting shows that without the central oxygen, the $Fe^{(III)}$ sites are $15e^-$ complexes, and the $Fe^{(II)}$ site is a $16e^-$ complex. This means that to satisfy the $18e^-$ rule for the three iron sites, all the valence electrons of the central oxygen must be involved in bonding.

The room temperature structure is as reported recently by Wu et al.[3y] In Table 2, selected bond lengths are given. The room-temperature structure has one Fe-O bond length typical of $Fe^{(III)}$ and two Fe-O bond lengths that are intermediate between $Fe^{(III)}$ and $Fe^{(II)}$ values. For this type of mixed-valence compound, there are several possible explanations of the two intermediate bond lengths: disorder, either static or dynamic, or electron delocalization. Using crystallographic data at only one temperature, it is difficult to distinguish these cases. However, as noted by Wu et al.,[3y] the anisotropy and orientation of the Fe thermal ellipsoids may provide valuable information on the nature of the system. Additional evidence from IR studies[3y] show that, on an IR time scale, the valence is localized. On the basis of multi-temperature Mössbauer data recorded between 8 and 298 K, Wu et al. suggested that a phase transition takes place between 96 and 101 K.[3y] They proposed that below the phase transition temperature, two structurally distinct molecules are present, both of which have fully localized electronic configurations $Fe^{(III)}Fe^{(III)}Fe^{(II)}$. In the high-temperature phase, only one molecule with fast intramolecular ET between two out of three iron sites is present, thus giving rise to the dynamically disordered crystal structure that is found from

(16) Koritsanszky, T.; Howard, S.; Mallinson, P. R.; Su. Z.; Richter, T.; Hansen, N. K. XD program; Institute of Crystallography, Freie Universität: Berlin, 1995.

(17) Flack, H. D.; Bernadinelli, G. *Acta Crystallogr. Sect A.* **1999**, *55*, 908−915.

Table 2. Selected Bond Lengths (Å)[a]

	temp (K)											
	10	28	35	60	85	100	118	135	160	200	240	295
Fe1-O1	2.040(6)	2.046(1)	2.037(3)	1.989(6)	1.964(2)	1.925(2)	1.922(2)	1.896(2)	1.898(2)	1.897(2)	1.909(3)	1.914(3)
Fe2-O1	1.824(6)	1.835(1)	1.827(3)	1.842(5)	1.832(2)	1.834(2)	1.836(2)	1.837(2)	1.837(2)	1.841(2)	1.844(3)	1.855(3)
Fe3-O1	1.862(6)	1.857(1)	1.859(3)	1.886(6)	1.922(2)	1.962(2)	1.971(2)	1.989(2)	1.997(2)	1.986(2)	1.965(3)	1.951(3)
Fe1-N(py)	2.199(7)	2.196(2)	2.190(4)	2.208(7)	2.208(2)	2.225(2)	2.234(3)	2.243(2)	2.243(3)	2.257(3)	2.243(4)	2.247(4)
Fe2-N(py)	2.235(7)	2.240(2)	2.230(4)	2.249(7)	2.240(2)	2.244(2)	2.246(3)	2.245(2)	2.252(3)	2.251(3)	2.251(4)	2.256(5)
Fe3-N(py)	2.237(8)	2.245(2)	2.230(4)	2.226(8)	2.223(2)	2.215(2)	2.216(3)	2.209(2)	2.217(3)	2.213(3)	2.219(4)	2.230(4)
⟨Fe1-O(piv)⟩	2.106	2.114	2.111	2.084	2.082	2.070	2.068	2.057	2.059	2.056	2.056	2.060
⟨Fe2-O(piv)⟩	2.035	2.036	2.033	2.024	2.032	2.032	2.032	2.031	2.032	2.031	2.025	2.031
⟨Fe3-O(piv)⟩	2.036	2.049	2.044	2.048	2.062	2.071	2.075	2.081	2.089	2.080	2.075	2.065

[a] ⟨Fe-O⟩ refers to the average over four bond lengths. Py = pyridine, piv = pivalate.

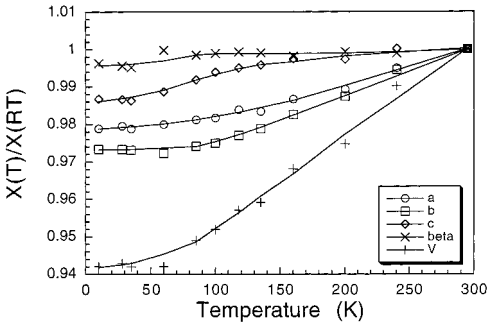

Figure 2. Unit-cell parameters relative to room-temperature values as a function of temperature. The lines serve as guides to the eye.

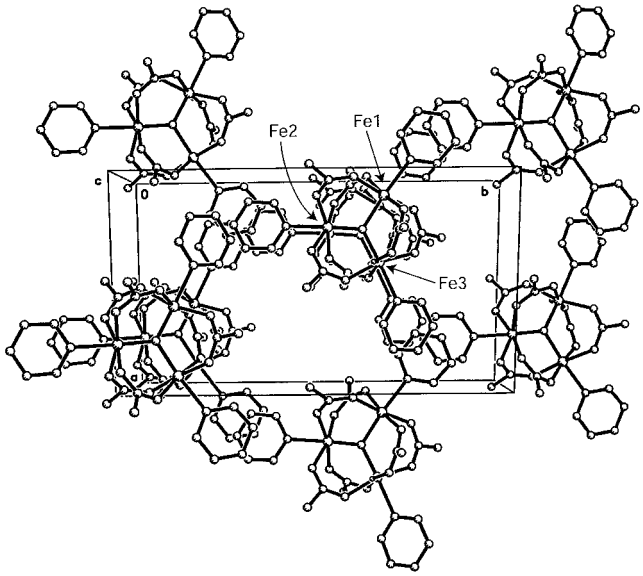

Figure 3. Packing diagram viewed along the *c*-axis. The *tert*-butyl groups and all the hydrogen atoms have been omitted for clarity.

room-temperature X-ray diffraction data.[3y] In the present study, we found that the space group of the crystal structure remains $P2_1$ throughout the entire temperature range (10−295 K). It should be stressed that one very extensive data set was recorded using an area detector technique with intense synchrotron radiation at very low temperature (28 K), and even under these conditions, we were unable to detect any changes in the space group. According to the crystallographic data, there is, therefore, only one structurally distinct molecule at all temperatures, and no specific change in the structure is observed between 96 and 101 K. Thus, the interpretation of the Mössbauer data is not supported by the temperature-resolved single-crystal data. As mentioned above, we do, however, observe a broadening of the diffraction peaks on cooling below 85 K. In Figure 2, the unit-cell parameters are plotted as a function of temperature. The plot supports that the structure does not go through any first- or second-order phase transitions, in accordance with the observed conservation of the space group over the entire temperature regime. It is notable that the unit cell contracts the least in the *c*-axis direction. In Figure 3 a packing diagram view along the *c*-axis of the structure is shown in which the *tert*-butyls that fill the voids have been omitted for clarity. The $\pi-\pi$ interactions between the pyridine ligands stacked along the *c*-axis probably restrain the crystal expansion in this direction, although it should be noted that consecutive pyridine molecules are not really coplanar, forming angles of 20−40°, and the interplanar distance is fairly long (∼3.5 Å).[18] The closest intermolecular contact is around 3 Å (H···H). The lack of phase transitions is further corroborated by DSC measurements between 100 K and room temperature, which show no thermal anomalies.

Variable-temperature crystallographic studies allow assessment of disorder and give information on the structural changes and phase transitions that occur upon cooling. The structures reported here show that considerable structural changes occur with temperature, and this strongly suggests that the system is disordered. The Fe-μ^3-O bond lengths (Figure 4a), perhaps best illustrate the dramatic changes that occur on cooling. In contrast to the Fe2−O1 bond length, which is almost temperature invariant and typical of an $Fe^{(III)}$-O separation, the Fe1−O1 and Fe3−O1 bond lengths are strongly temperature-dependent. From room temperature to 160 K, the Fe3−O1 bond length increases slightly from 1.951(3) Å to 1.997(2) Å, whereas the Fe1−O1 bond length decreases from 1.914(3) Å to 1.898(2) Å. Around this temperature, a change occurs, and as the temperature is further lowered, the Fe3−O1 bond length instead decreases, and Fe1−O1 increases. At 10 K, Fe3−O1 is 1.862(5) Å, which is typical of an $Fe^{(III)}$−O bond, and Fe1−O1 is 2.040(6) typical of an $Fe^{(II)}$−O bond. In other words, the system appears to be close to valence-trapped at 10 K, although a small difference in the $Fe^{(III)}$-O1 bond lengths persists [1.862(5) Å versus 1.824(6) Å]. Similar changes are observed for the Fe-O(pivalate) bond lengths (Figure 4b). Although the changes are smaller, the overall pattern is similar to that observed for the Fe-μ^3-O bond lengths. The Fe-N(pyridine) bond lengths, which are trans to the Fe-μ^3-O bonds, also show a slight temperature variation, but the changes appear to be in the sense opposite to those involving oxygen (Figure 4c). Thus, the iron sites with the shorter Fe-O bond lengths have the longer Fe-N bond lengths and vice versa.[19] It is encouraging to observe that even though Figure 4a−c is based on measurements of five different crystals under very different experimental conditions, there is good

(18) In the room temperature study by Wu et al.,[3y] the shortest pyridine−pyridine contact was erroneously reported to be >6 Å.

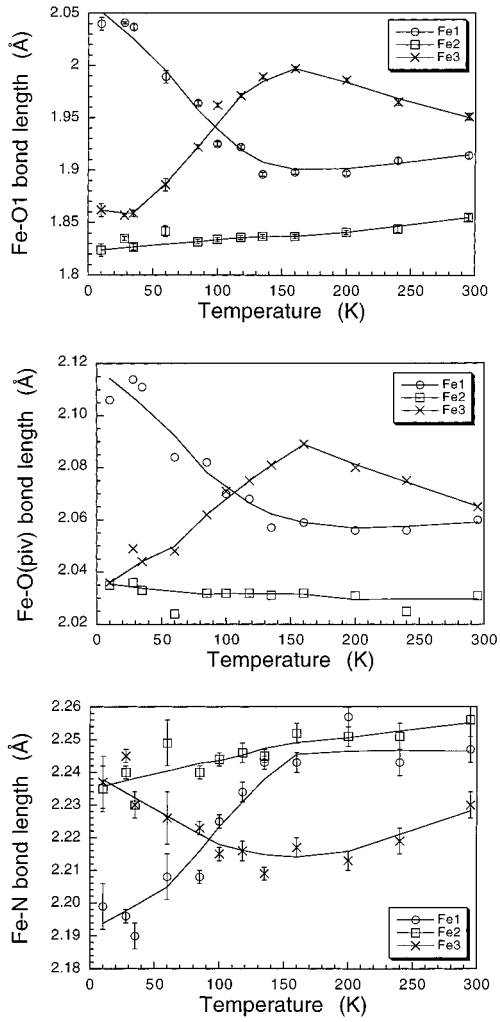

Figure 4. Metal-to-ligand bond lengths as a function of temperature: (a) Fe-O(μ^3) bond lengths with error bars corresponding to 1 standard uncertainty (su), (b) average Fe-O (pivalate) bond lengths, (c) Fe-N (pyridine) bond lengths with error bars corresponding to 1 su. The lines serve as guides to the eye.

agreement between the studies. Thus, it is, for example, observed that the parameters derived from the 28 K synchrotron data agree well with the parameters derived from the 35 K conventional data. This suggests that systematic errors in the results are relatively small.

The present study is a good example of the power of very low-temperature crystallography. With a conventional liquid nitrogen cryostat, data cannot be measured below 90−100 K. If we had only known the structural features above 100 K, we would have missed completely the valence-trapping process that is seen in Figure 4. The very low-temperature X-ray data furthermore contradict structural suggestions based on indirect measurements using spectroscopic methods. The clear change in the Mössbauer data between 96 and 101 K, therefore, must have another origin.[3y] However, it is conspicuous that the suggested phase-transition temperature corresponds closely to

(19) For the extensive 28 K synchrotron data, use of a complete multipole electron density model affects the Fe1-N and Fe1-O1 bond lengths considerably, whereas the other bonds lengths are relatively unchanged. Thus, Fe1-N increases to 2.231(2) Å, and Fe1-O1 decreases to 2.007(2) Å. This may be related to phase uncertainties in an acentric crystal structure or perhaps a thermally accessible excited state. The effect does not affect the main conclusions of the paper. For consistency, all data sets are treated with the same spherical-atom model.

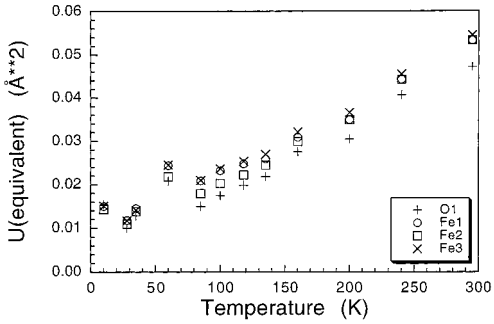

Figure 5. Equivalent isotropic atomic displacement parameters for the central Fe and O atoms.

the crossover temperature of the two Fe-μ^3-O bond lengths, although no connection between the two phenomena has been found.

3.2 Analysis of Atomic Displacement Parameters

If the system is disordered, then the structural changes can be explained by an ET process taking place between the iron atoms. At higher temperatures, the structure has an average $Fe^{(II)}$ and $Fe^{(III)}$ geometry at the sites involved in the transfer. As the temperature is decreased, a lowest energy configuration of trapped $Fe^{(III)}Fe^{(III)}Fe^{(II)}$ geometry is reached. This type of valence trapping process is well-documented for trinuclear oxo-bridged complexes (see ref 3 and references therein). However, with the exception of only one example,[3v] $[Fe_3O(O_2C-CH_2Cl)_6(H_2O)_3)]\cdot 3H_2O$, the valence trapping has involved all three Fe sites, that is, the exchange is $Fe^{(III)}Fe^{(III)}Fe^{(II)} \leftrightarrow Fe^{(III)}Fe^{(II)}Fe^{(III)} \leftrightarrow Fe^{(II)}Fe^{(III)}Fe^{(III)}$. Evidently, the present system only involves two of these processes, because the Fe2 position appears completely occupied by an $Fe^{(III)}$ atom over the whole temperature range.

To further examine the disorder, we turn to analysis of the atomic displacement parameters (ADPs). In Figure 5 the equivalent isotropic mean square displacement amplitudes of the central atoms are shown as a function of temperature. The ADPs have the expected temperature dependence, and near 10 K, they change little. It is clear from the plot that the 60 K values, and to a smaller extent the 10 K values, are outliers as compared with the other data. However, because the positional parameters (and the derived bond lengths) agree reasonably well with the other data (see Figure 4), it seems that the 10 and 60 K data suffer from an uncorrected systematic error which has largely been absorbed in the ADPs. This could be due to scan truncation that was caused by the large crystal mosaicity observed for crystal 1 below 85 K. It could also be due to inadequate temperature control, whereas it is unlikely to be extinction or absorption effects which are constant for a given crystal. In further analysis of the ADPs, we omitted the 60 K data.

Analysis of ADPs has been used in many studies of structural disorder,[20] including analysis of dynamic Jahn−Teller distortions.[21] Bürgi and co-workers have pointed out that studies of *difference* ADPs are less affected by systematic errors such as extinction, absorption, and thermal diffuse scattering and, thus,

(20) (a) Dunitz, J. D.; Schomaker, V.; Trueblood, K. N. *J. Phys. Chem.* **1988**, *92*, 856−867. (b) Dunitz, J. D.; Maverick, E. F.; Trueblood, K. N. *Angew. Chem., Int. Ed. Engl.* **1988**, *27*, 880−895. (c) Madsen, G. K. H.; Iversen, B. B.; Larsen, F. K.; Kapon, M.; Reisner, G.; Herbstein, F. H. *J. Am. Chem. Soc.* **1998**, *120*, 10040−10045.

(21) (a) Ammeter, J. H.; Bürgi, H. B.; Gamp, E.; Meyer-Sandrin, V.; Jensen, W. P. *Inorg. Chem.* **1979**, *18*, 733−750. (b) Wood, J. S.; Keijzers, C. P.; Boer, E.; Buttafava, A. *Inorg. Chem.* **1980**, *19*, 2213−2225. (c) Hathawat, B. J. *Coord. Chem. Rev.* **1981**, *35*, 211−252. (d) Simmons, C.

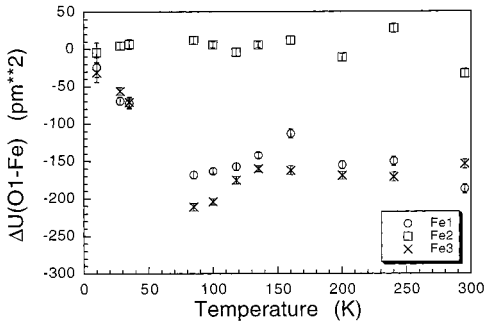

Figure 6. Difference-atomic-displacement parameters along the μ^3-O-Fe bond directions.

provide sensitive measures of dynamic processes in crystals.[22] If the iron atoms are disordered over two positions corresponding to $Fe^{(II)}$ and $Fe^{(III)}$, respectively, then the ADPs of the iron atoms should have an extra component along the Fe-μ^3-O bond direction which is not due to actual thermal motion. In Figure 6 the differences between the μ^3-oxygen and iron mean square displacements along the bond directions are plotted as a function of temperature. For covalent bonds in typical organic molecules, which can be assumed to be fairly rigid, these differences should be small (<10 pm^2) if no disorder is present.[23] On the other hand, metal-ligand bonds are less rigid, and they typically have difference ADPs around 10−30 pm^2. Figure 6 clearly demonstrates the disordered nature of the system. While the ΔU values along the Fe2-μ^3-O bond are very small at all temperatures, the values along the Fe1-μ^3-O and Fe3-μ^3-O are very large. This shows that the Fe2 site is structurally ordered relative to the μ^3-oxygen, whereas the Fe1 and Fe3 are disordered. As the temperature becomes very low, the disorder freezes out, and at 10 K, all of the Fe sites appear ordered. The low value of ΔU(O1-Fe2) shows that either both sites are ordered or they behave as a rigid entity in the disordered structures. It is still conceivable that the μ^3-oxygen has some disorder perpendicular to the Fe2-μ^3-O bond direction in the Fe3-O plane. Such μ^3-oxygen disorder would be due to the varying bond lengths to Fe1 and Fe3, which is dependent on their valence states. However, at all temperatures, the thermal ellipsoid of the μ^3-oxygen is close to isotropic, and furthermore, the temperature dependence of the thermal parameters (Figure 5) shows no anomalies except for the 10 and 60 K values, which have been accounted for. Therefore, it appears that the μ^3-oxygen is structurally ordered. The fact that the disorder only involves the Fe1 and Fe3 sites substantiates that the intramolecular electron transfer takes place through vibronic coupling that is dominated by molecular distortion mode, Q_v in the notation of Kambara et al., for the isolated molecule.[24]

3.3 Potential Energy Surface. A number of studies have attempted to develop theoretical models for the potential energy surface (PES) of trinuclear oxo-bridged systems.[24] The isolated $[Fe_3O(O_2CR)_6(L)_3]$ system presumably has either three or four potential minima, depending on the exact nature of the complex. Three of these minima are equal in energy and correspond to localization of the "extra" d electron at each of the three Fe sites (Figure 7a). The fourth minimum, which is present in complexes with strong vibronic coupling, corresponds to an undistorted trinuclear core in which the electron is delocalized over all three sites. If the thermal energy of the system is larger than the potential barrier for electron transfer, the system also has a delocalized structure. For a molecule in a crystal, there are interactions with the surroundings, and if the symmetry of the crystal is different from that of the individual molecules, then the three iron sites become nonequivalent, (Figure 7b). The stronger the interaction with the crystal field, the larger the energy difference between the minima may become.

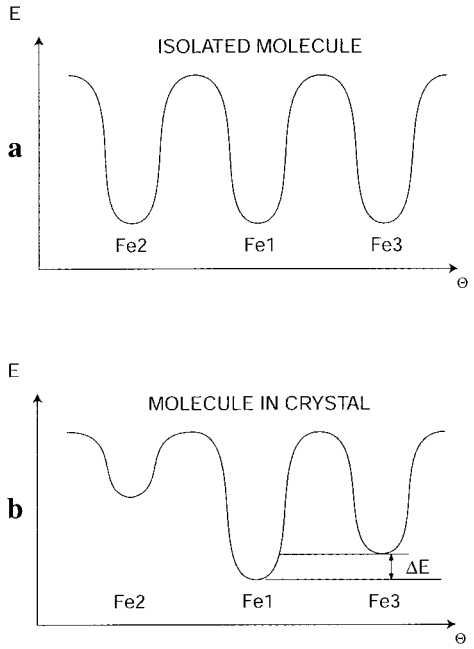

Figure 7. Sketch of the idealized potential energy surface for an isolated molecule (a) and for a molecule in a crystal (b). Each minimum corresponds to localization of the "extra" d electron at the labeled atom.

The PES of the trinuclear complexes resembles that of dynamic Jahn−Teller distorted octahedral complexes.[25] A large amount of literature exists concerning dynamic Jahn−Teller distorted complexes,[21] and in such systems, temperature-resolved structural data have been used to derive the energy difference between potential minima.[26] If we assume that in the present complex, one iron site remains valence-trapped at all temperatures (Fe2 = $Fe^{(III)}$), then the apparent Fe1-O1 and Fe3-O1 bond lengths at any given temperature may be, in a first approximation, due to a Boltzmann-weighted population of the two lowest-lying minima. If P_I is the population of the first minimum and P_{II} is the population of the second minimum, we have $P_I/P_{II} = \exp(\Delta E/kT)$. We now define $d_{obs} = |\text{Fe1-O1}| - |\text{Fe3-O1}|$ at any given temperature and d_{max} as the value obtained for the ordered low-temperature structure. The energy difference between the two minima can then be written as $\Delta E = kT \ln[(d_{max} + d_{obs})/(d_{max} - d_{obs})]$. At low temperatures (10, 28, and 35 K) an ordered state is reached with constant Fe-O bond length (see Table 2). Because the synchrotron data recorded at 28 K are the more accurate, we used these data to define $d_{max} = 0.184$ Å. In Figure 8, $\ln[(d_{max} + d_{obs})/(d_{max} - d_{obs})]$ is plotted against $1/T$. The Boltzmann model breaks down at the crossover

J.; Hathaway, B. J.; Amornjarusiri, K.; Santarsiero, B. D.; Clearfield, A. *J. Am. Chem. Soc.* **1987**, *109*, 1947−1958. (e) Stebler, M.; Bürgi, H. B. *J. Am. Chem. Soc.* **1987**, *109*, 1395−1401. (f) Simmons, C. J. *New J. Chem.* **1993**, *17*, 77−95.

(22) Chandrasekhar, K.; Bürgi, H. B. *Acta Crystallogr. Sect B* **1984**, 387−397.

(23) Hirsfeld, F. L. *Acta Crystallogr. Sect. A* **1976**, *32*, 239−244.

(24) (a) Kambara, T.; Hendrickson, D. N.; Sorai, M.; Oh, S. M. *J. Chem. Phys.* **1986**, *85*, 2895−2909. (b) Cannon, R. D.; Montri, L.; Brown, D. B.; Marshall, K. M.; Elliott, C. M. *J. Am. Chem. Soc.* **1984**, *106*, 2591−2594.

(25) Bersuker, I. B. *Eletronic Structure and Properties of Transition Metal Compounds: Introduction to the Theory*; Wiley: New York, 1996.

(26) (a) Alcock, N. W.; Duggan, M.; Murray, A.; Tyagi, S.; Hathaway, B. J. *J. Chem. Soc., Dalton Trans.* **1984**, 7−14. (b) Iversen, B. B.; Larsen, F. K.; Reynolds, P. A.; Figgis, B. N. *Acta Chem. Scand.* **1994**, *48*, 800−809.

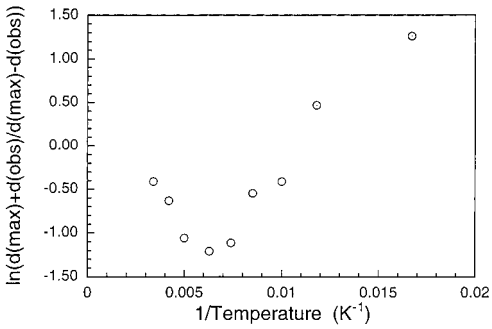

Figure 8. $\ln[(d_{max} + d_{obs})/(d_{max} - d_{obs})]$ versus reciprocal temperature; d_{max} is taken as 0.184 Å (the 28 K value).

temperature of the two Fe-O bond lengths (~95 K) because above the crossover temperature, the model would imply that the higher energy minimum is more populated than the lower minimum. Some other effect must be responsible for the increased population of the higher minimum. Therefore, we can use the data points only at 60 and 85 K to estimate the energy difference between the minima, and this gives $\Delta E = 44$ cm^{-1}. Considering the uncertainty of the applied model, it is probably only reasonable to state that ΔE is below 100 cm^{-1}.

It is conceivable that the whole PES is changing with temperature, that is, ΔE is temperature-dependent. This could explain the paradox of the higher minimum being more populated than the lower minimum above the crossover temperature. In case of a temperature-dependent PES, the order of the two minima is reversed at the crossover temperature. However, a continuous change of the PES with temperature would appear to necessitate a structural change with temperature. As mentioned above, we have been unable to detect any DSC signal between 100 and 295 K, and the cell parameters also do not show obvious evidence of structural changes. With increasing temperature, the most conspicious change in the structure is the onset of *tert*-butyl disorder. At low temperatures, the best structural model contains single carbon sites with anisotropic thermal parameters, whereas at higher temperatures the *tert*-butyl carbon atoms are clearly disordered over two sites, as seen in Figure 9. The *tert*-butyl disorder may be the origin of a gradual change in the PES with temperature, and therefore, it indirectly affects the ET process. Because not all of the methyls get disordered simultanously, the process is broad in temperature, and this can explain the lack of thermal anomaly in the DSC data. A clear phase transition due to onset of *tert*-butyl disorder has been observed by Asamaki et al. for $[Fe_3O(O_2CC(CH_3)_3)_6\ (CH_3)_3CCO_2H)_3]$.[3u]

It is difficult to differentiate between crystallographic models of *tert*-butyls having two disordered carbon sites with isotropic thermal motion and a single site with anisotropic thermal motion. A single-site anisotropic model often gives a lower *R* factor than a two-site isotropic model, and furthermore, a two-site anisotropic model is unstable in the refinements. However, the *tert*-butyl disorder presumably involves a PES with a rotational barrier between two fixed sites. Because the disorder is most prominent at room temperature, we have used these data to refine the positions of the sites. In refinements at the other temperatures, the distance between the disordered carbons was held fixed through a soft restraint, and only the occupancies of the two sites and a common isotropic thermal parameter for each *tert*-butyl group was varied. The refined occupancies are probably accurate only when the occupation of the minor component is more than 10−15%. Table 4 lists the occupancies of the major component of each *tert*-butyl group as a function

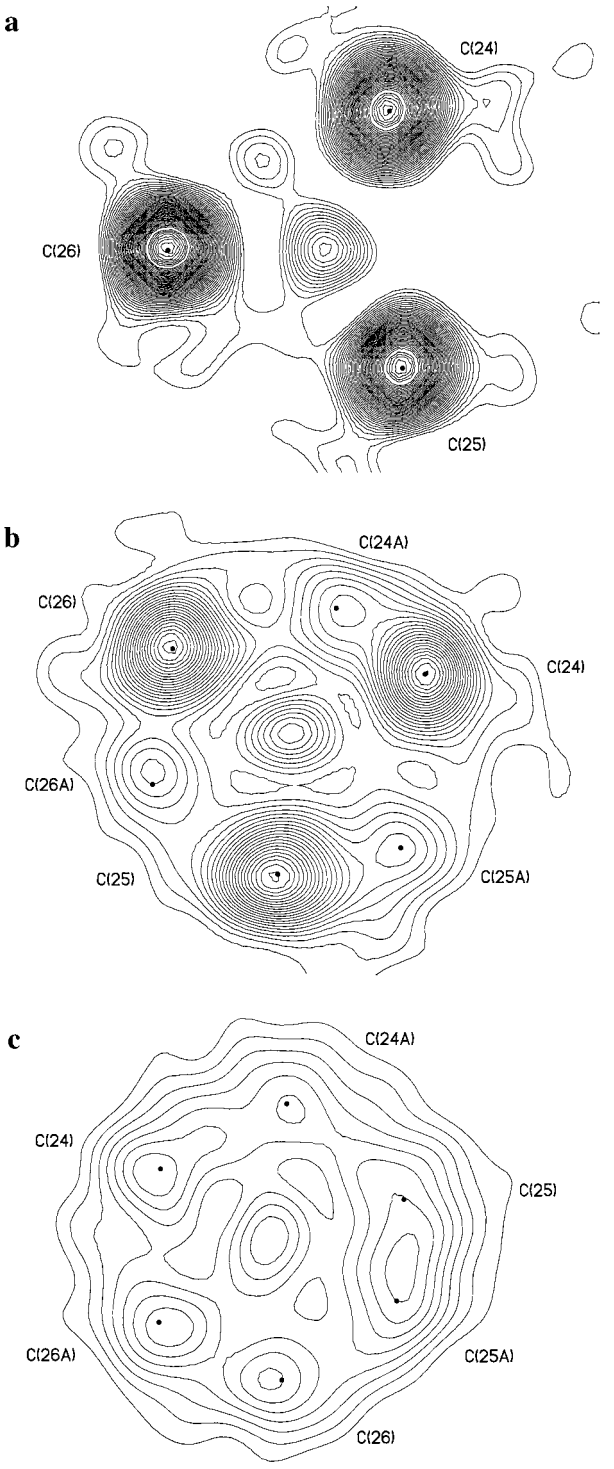

Figure 9. Difference Fourier maps through the plane of the methyl carbons of the *tert*-butyl group involving C23: (a) 10 K, (b) 135 K, and (c) 295 K.

of temperature. At room temperature, all except one of the *tert*-butyl groups are disordered approximately in a ratio 50:50. As the temperature is lowered, one *tert*-butyl gets fully ordered just below 150 K, and around 85 K the disorder of the four remaining *tert*-butyls freezes out. The ordering of the *tert*-butyls may well increase the internal stress in the crystal and, therefore, be the origin of the increase in mosaicity observed around 85 K. This is further substantiated by the fact that the effect is reversible. The refined *tert*-butyl occupancies validate that below 85 K, the PES is temperature-invariant, and thus, we are justified

Table 3. Atomic Displacements Parameters (pm^2)

	temp (K)											
	10	28	35	60	85	100	118	135	160	200	240	295
U_{eq}(O1)	154(13)	100(5)	129(7)	208(11)	150(5)	175(4)	199(5)	219(4)	276(6)	305(5)	407(6)	472(6)
U_{eq}(Fe1)	150(3)	145(1)	145(2)	244(3)	209(1)	232(1)	248(1)	259(1)	309(1)	349(1)	443(2)	533(2)
U_{eq}(Fe2)	143(3)	138(1)	138(2)	219(3)	179(1)	203(1)	223(1)	245(1)	299(1)	349(1)	445(2)	542(2)
U_{eq}(Fe3)	151(3)	141(1)	141(2)	245(3)	210(1)	237(1)	254(1)	270(1)	321(1)	366(1)	455(2)	545(2)
ΔU(O1-Fe1)	−24(13)	−69(5)	−72(7)	−90(11)	−168(5)	−163(4)	−157(5)	−142(4)	−113(6)	−155(5)	−150(6)	−187(6)
ΔU(O1-Fe2)	−4(13)	5(5)	7(7)	−58(11)	12(5)	6(4)	−4(5)	6(4)	12(6)	−11(5)	28(6)	−33(6)
ΔU(O1-Fe3)	−31(13)	−56(5)	−71(7)	−94(11)	−211(5)	−204(4)	−175(5)	−160(4)	−162(6)	−169(5)	−171(6)	−154(6)

Table 4. Occupancies of the Major *tert*-Butyl Components as a Function of Temperature

temp (K)	*P*(C13)	*P*(C23)	*P*(C33)	*P*(C43)	*P*(C53)	*P*(C63)
60 and below	1.00	1.00	1.00	1.00	1.00	1.00
85	0.910(5)	0.898(5)	0.939(6)	1.00	1.00	1.00
100	0.884(5)	0.846(5)	0.897(6)	1.00	0.940(6)	1.00
118	0.892(6)	0.832(6)	0.892(7)	1.00	0.924(7)	1.00
135	0.845(5)	0.734(6)	0.814(6)	1.00	0.855(7)	1.00
160	0.822(5)	0.682(5)	0.767(6)	0.910(6)	0.779(6)	1.00
200	0.767(6)	0.590(7)	0.669(7)	0.829(7)	0.570(6)	1.00
240	0.653(6)	0.536(6)	0.565(7)	0.763(6)	0.559(6)	1.00
295	0.626(7)	0.500(7)	0.569(8)	0.700(7)	0.514(6)	1.00

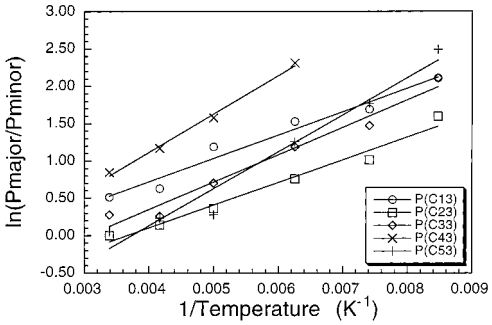

Figure 10. Plot of $\ln(P_{minor}/P_{major})$ against reciprocal temperature. The slope is $\Delta E/k_B$. Only data points above 100 K have been used to estimate ΔE. The refined linear relations are $y(C13) = 313.9x - 0.536$ ($R^2 = 0.97$); $y(C23) = 304.6x - 1.113$ ($R^2 = 0.98$), $y(C33) = 367.8x - 1.123$ ($R^2 = 0.97$), $y(C43) = 515.9x - 0.949$ ($R^2 = 0.99$), $y(C53) = 496.4x - 1.853$ ($R^2 = 0.96$).

in applying the Boltzmann model as an explanation for the observed changes in Fe-μ^3-O bond lengths. The *tert*-butyl occupancies can also be used directly to estimate the energy difference between the disordered structures. Thus, if we plot $\ln(P_{minor}/P_{major})$ against $1/T$, the slope will be $\Delta E/k_B$ (Figure 10). The energy differences are 217, 212, 255, 359, and 345 cm^{-1} for the *tert*-butyl groups containing C13, C23, C33, C43, and C53, respectively.

It is puzzling why the Fe2 site remains valence-trapped at all temperatures. In other words, what makes the Fe2 minimum on the PES sit at a higher energy than the two others? The most obvious asymmetry in the molecule is the C63 *tert*-butyl group, which is ordered at all temperatures. This *tert*-butyl group is situated opposite to the Fe2 atom. Thus, it clearly breaks the mirror planes between Fe1 and Fe2 and between Fe3 and Fe2 but not between Fe1 and Fe3. The most striking structural change with temperature is the reversal in the trend of the Fe1-O1 and Fe3-O1 bond lengths around 150 K (Figure 4). Above 150 K, the system seems to approach a configuration in which the extra d electron is trapped at Fe3, but below 150 K, it is, instead, the Fe1 position which becomes an $Fe^{(II)}$ site. The change must be related to subtle energy changes in the crystal, because there are no phase transitions around this temperature. There are two structural features which change near 150 K. First, the C43 *tert*-butyl group becomes ordered upon cooling below 150 K (Table 4) and, second, the *c*-axis starts contracting slightly faster around this temperature (Figure 2). The ordering of the C43 *tert*-butyl group, which is located opposite to Fe1, makes Fe3 the "odd" iron center of the structure. As with the uniqueness of Fe2 above 150 K, this may cause a relative increase of the Fe3 PES minimum, which eventually causes Fe3 to become trapped as $Fe^{(III)}$ at 10 K. The C43 *tert*-butyl ordering seems to allow for a larger contraction in the *c*-axis direction. The fact that the ordering of the *tert*-butyls is correlated to the forces acting along the *c*-axis suggests that it is the requirements of the *tert*-butyls which, at least to some extent, prevent the pyridines from being coplanar with the central Fe_3O plane and, thereby, also prevent obtaining a good $\pi-\pi$ stacking along the *c*-axis. Overall, this demonstrates that for **1**, the dynamic behavior of the *tert*-butyls strongly affects the intramolecular ET process. In the absence of a strong crystal field created, for example, by a dense packing or by solvent molecules, very fine energy changes can have large structural effects.

3.4 The Crystal Field. As documented in refs 2 and 3 (and references therein), a very considerable number of mixed-valence Fe_3O compounds have been studied. A search in the Cambridge Structural Database reveals 81 Fe-μ^3-O bond lengths, which are plotted in Figure 11. Clearly, the majority of the $[Fe_3O(RCOO)_6L_3]\cdot n$S structures appear to be intermediate in valence, with very few structures being trapped at two $Fe^{(III)}-O$ and one $Fe^{(II)}-O$ bond lengths. The present very low-temperature structures (10, 28, and 35 K) have the widest span of Fe-μ^3-O bond lengths observed so far. This demonstrates the effect of very low temperatures in valence-trapping the structures, and suggests that many crystal structures could be rewardingly reexamined at very low temperatures to better appreciate important physical effects such as intramolecular ET.

There exists only one other study of trinuclear iron compounds that were resolved structurally at more than two temperatures. This is a study by Hendrickson and co-workers on $[Fe_3O(O_2CCH_3)_6(3\text{-Cl-py})]\cdot 3\text{-Cl-py}$.[3r] This structure has extra solvent molecules present in the crystal, and therefore, we expect that the crystal forces to be stronger in that system. In **1,** the intermolecular contacts are long and consist of weak H··· H interactions (∼3 Å). Furthermore, there are no solvent molecules in the crystal. The $[Fe_3O(O_2CCH_3)_6(3\text{-Cl-py})]\cdot 3\text{-Cl-py}$ structure

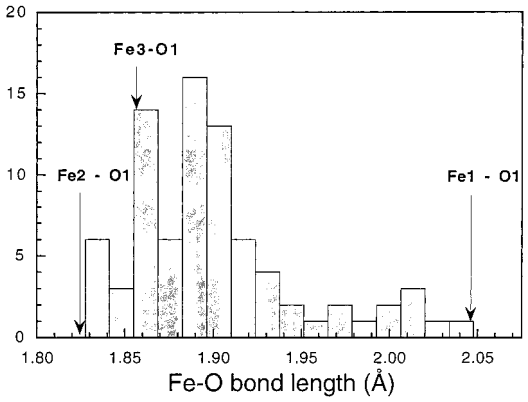

Figure 11. Histogram over reported Fe-μ^3-O bond lengths in mixed-valence trinuclear carboxylate compounds. The present 28 K Fe-μ^3-O bond lengths are indicated with arrows.

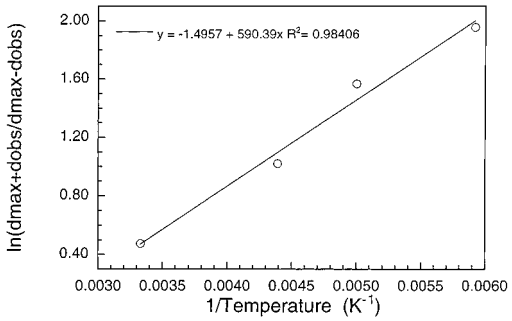

Figure 12. $\ln[(d_{max} + d_{obs})/(d_{max} - d_{obs})]$ versus reciprocal temperature for $[Fe_3O(O_2CCH_3)_6(3\text{-Cl-py})]\cdot 3\text{-Cl-py}$.[3r]

has two equivalent Fe sites, but the third is different. The PES, therefore, presumably has two identical minima and a third minimum at a different energy. Thus, we can use the Boltzmann population model that is described above to calculate the energy difference between the two potential minima. In Figure 12, the plot corresponding to Figure 8 is shown on the basis of the data reported in the original publication.[3r] Linear regression gives $\Delta E = 410\ cm^{-1}$. The intercept of the line with the ordinate is different from zero. This has also been observed in several studies of dynamic Jahn−Teller distorted systems,[21f] and it is an indication that the simple Boltzmann model is not fully adequate. The much larger value of ΔE obtained for $[Fe_3O(O_2CCH_3)_6(3\text{-Cl-py})]\cdot 3\text{-Cl-py}$ than that obtained for **1** reflects the stronger crystal field on the molecule. Hendrickson and co-workers have also studied $[Fe_3O(O_2CCH_3)_6(C_5H_5N)_3]$, which is very similar to **1**.[3f] That structure, which contains acetate instead of pivalate bridges, was reported to be valence-trapped even at 315 K. In **1,** the steric requirements of the bulky pivalate ligands create an open structure having weak intermolecular interactions. In contrast to this, the stronger intermolecular interactions in the more densely packed acetate-bridged complex creates a much larger ΔE value and results in a valence-trapped complex even at elevated temperatures.

Conclusion

Multi-temperature X-ray crystallographic data on $[Fe_3O(O_2CC(CH_3)_3)_6(C_5H_5N)_3]$ has revealed that at very low temperatures (10 K), the system becomes valence-trapped in a single ordered configuration. The interpretation of the temperature-dependent bond lengths in the form of a disorder model is strongly supported by analysis of the ADPs. The difference ADPs exhibit a large excess along the Fe-μ^3-O bond directions at higher temperatures for two of the iron atoms. The use of a Boltzmann model for thermal population of the two lowest-lying minima on the PES of the structure allows the energy difference between the minima to be estimated, $\Delta E < 100\ cm^{-1}$. A similar model applied to literature data on $[Fe_3O(O_2CCH_3)_6(3\text{-Cl-py})]\cdot 3\text{-Cl-py}$ yields $\Delta E = 410\ cm^{-1}$. A Boltzmann population model applied to the disordered *tert*-butyl groups yields energy differences between the two disordered *tert*-butyl configurations of 217, 212, 255, 359, and 345 cm^{-1} for the groups containing C13, C23, C33, C43, and C53, respectively. The dynamic behavior of the *tert*-butyl groups appears to be a dominant factor that affects the intramolecular ET process of the system as well as the physical properties of the crystal (thermal expansion, mosaicity). In the absence of a strong crystal field due to a dense packing or solvent molecules, very fine energy changes can result in substantial structural rearrangements. The present study indicates that a number of previously published crystal structures of trinuclear complexes could be rewardingly reexamined at temperatures below the boiling point of nitrogen.

Acknowledgment. B.B.I. and S.P.P. are grateful to the Scientia Europaea Forum under the auspices of the French Academy of Science and the Rhône-Poulenc Foundation/Institut de France, without whom the present study would never have been initiated. C.W. thanks the DANSYNC center under the Danish Natural Science Research Council for a post-doctoral stipend. We thank Prof. Kurt Nielsen for assistance with the 118 K data collection at the Technical University of Denmark and Dr. Piero Macchi for helpful discussions. We also gratefully acknowledge the beam time obtained at beam line X3A1, the National Synchrotron Light Source, Brookhaven National Laboratory, U.S.A., for collection of the 28 K data. The SUNY X3 beam line at NSLS is supported by the Division of Basic Energy Sciences of the U.S. Department of Energy (DEFG0286ER45231).

Supporting Information Available: Crystallographic information files (CIF) for all data sets have been deposited at cif.ja@acs.org. This material is available free of charge via the Internet at http://pubs.acs.org.

JA994162A